Inorg. Chem. **2006**, *45*, 220–229

Synthesis, Characterization, Sintering, and Leaching of β-TUPD/Monazite Radwaste Matrices

N. Clavier and N. Dacheux*

Groupe de Radiochimie, Institut de Physique Nucléaire d'Orsay, Bât. 100, Université Paris-Sud-11, 91406 Orsay, France

R. Podor

Laboratoire de Chimie du Solide Minéral, Université H. Poincaré—Nancy I, BP 239, 54506 Vandoeuvre lès Nancy, France

Received September 19, 2005

To study the simultaneous incorporation of both tri- and tetravalent actinides in phosphate ceramics, we prepared several β-TUPD/monazite-based radwaste matrices through two different chemical routes (called dry and wet routes) involving the initial precipitation of crystallized precursors of each phase, i.e., TUPHPH solid solutions on the one hand, and rhabdophane ($LnPO_4 \cdot xH_2O$) on the other. The final material was obtained after heating above 1000 °C, and no additional phase was detected from elementary analyses and XRD. Moreover, the complete segregation of tri- and tetravalent cations was evidenced when using dry chemical processes. This method also allows for the preparation of dense pellets ($90\% < d_{exp}/d_{calc} < 95\%$) after only 10–20 h of heat treatment at 1250 °C. Finally, the chemical durability of the pellets was examined through several leaching experiments in acidic media. The normalized dissolution rate determined from the uranium release in the leachate varies from $(8.2 \pm 0.7) \times 10^{-6}$ to $(2.7 \pm 0.4) \times 10^{-2}$ g m^{-2} day^{-1} between 25 and 120 °C in 10^{-1} M HNO_3. Near equilibrium, thorium and lanthanide ions were found to quickly precipitate as phosphate-based neoformed phases in the back end of the initial dissolution process. These phases were identified as uranium-depleted T(U)PHPH and as rhabdophane or monazite.

1. Introduction

The immobilization of long-life radionuclides, such as actinides coming from the back end of the nuclear fuel cycle or from dismantled nuclear weapons, in an underground repository is actually one of the main options envisaged for managing high activity and long-life radioactive waste. In this field, the French research group NOMADE (CEA/CNRS/AREVA/EDF/French Universities) was set up to develop ceramic materials with several properties of interest, including high weight loading in actinides, good sintering capability, and strong resistance to aqueous alteration and radiation damage.[1,2] On this basis, four matrices were selected for a further extensive study: one titanate-based material, zirconolite ($CaZrTi_2O_7$),[3−5] and three phosphate-based materials, apatite ($Ca_{10}(PO_4)_6F_2$) and associated britholites ($Ca_9Nd_{1-x-y}An^{III}_yAn^{IV}_x(PO_4)_{5-x}(SiO_4)_{1+x}F_2$),[6,7] monazite ($LnPO_4$) and associated brabantites ($N^{II}M^{IV}(PO_4)_2$),[8−14] and

* To whom correspondence should be addressed. E-mail: dacheux@ipno.in2p3.fr.

(1) André, J. C. *C. R. Acad. Sci., Ser. IIa* **2001**, *333*, 835−839.
(2) Deschanels, X. *Evaluation de la Faisabilité Technique des Nouvelles Matrices de Conditionnement des Radionucléides à vie Longue*; Technical Report DTCD/2004/5; Commissariat à l'Energie Atomique (CEA)—Département d'Etudes du Traitement et du Conditionnement des Déchets (DTCD): Paris, 2004.
(3) Begg, B. D.; Vance, E. R.; Day, R. A.; Hambley, M.; Conradson, S. D. In *Scientific Basis for Nuclear Waste Management XX*; Material Research Society: Boston, 1997.
(4) Guy, C.; Audubert, F.; Lartigue, J. E.; Latrille, C.; Advocat, T.; Fillet, C. *C. R. Acad. Sci., Ser. IIb* **2002**, *3*, 827−837.
(5) Advocat, T.; Fillet, C.; Marillet, J.; Leturcq, G.; Boubals, J. M.; Bonnetier, A. In *Scientific Basis for Nuclear Waste Management XXI*; Material Research Society: Boston, 1998.
(6) Carpena, J.; Audubert, F.; Bernache, D.; Boyer, L.; Donazzon, B.; Lacout, J. L.; Senamaud, N. In *Scientific Basis for Nuclear Waste Management XXI*; Material Research Society: Boston, 1998.
(7) Bros, R.; Carpena, J.; Sere, V.; Beltritti, A. *Radiochim. Acta* **1996**, *74*, 277−282.
(8) Boatner, L. A.; Sales, B. C. *Radioactive Waste Forms for the Future*; North-Holland Physics Publishing: Amsterdam, 1998.
(9) Montel, J. M.; Devidal, J. L.; Avignant, D. *Chem. Geol.* **2002**, *191*, 89−104.
(10) Podor, R.; Cuney, M. *Am. Mineral.* **1997**, *82*, 765−771.

10.1021/ic051607p CCC: $33.50
Published on Web 11/30/2005

thorium phosphate−diphosphate solid solutions (β-$Th_{4-x}An_x(PO_4)_4P_2O_7$).[15−20]

Several matrices allow for the simultaneous incorporation of tri- and tetravalent actinides: zirconolite ($Ca_{1-x}An^{III}_xZr_{1-y}An^{IV}_yTi_{2-x}Al_xO_7$),[3] britholite ($Ca_9Nd_{1-x-y}An^{III}_yAn^{IV}_x(PO_4)_{5-x}(SiO_4)_{1+x}F_2$),[21] and monazite/brabantite solid solutions ($La_{1-x-2y}An^{III}_xCa_yAn^{IV}_y(PO_4)_2$).[22] Preliminary works concerning the elaboration of britholites of the general formula $Ca_9Nd_{1-x}An^{IV}_x(PO_4)_{5-x}(SiO_4)_{1+x}F_2$ (An^{IV} = Th, U) show that thorium can be incorporated up to 20 wt % in the material whereas it is limited to 8 wt % for uranium.[23] In this formula, trivalent actinides can be simulated by neodymium.[24] The existence of a complete solid solution between monazite and brabantite[22] seems suitable for the incorporation of actinides of different oxidation states in a unique matrix. Nevertheless, the incorporation of tetravalent cations in the brabantite structure could appear complex because of redox reactions, as for plutonium(IV), and steric constraints. Indeed, the restrictions driving the substitution in monazite are the following[22]

$$1.238 \geq \frac{^{IX}r_{M^{2+}}}{^{IX}r_{M^{4+}}} \geq 1.082 \qquad (1)$$

$$1.216\ \text{Å} \geq \frac{^{IX}r_{M^{2+}} + {}^{IX}r_{M^{4+}}}{2} \geq 1.100\ \text{Å} \qquad (2)$$

In the same way, the elaboration of β-TPD/monazite-based radwaste matrices could allow for the incorporation of large amounts of both trivalent (in the monazite structure) and tetravalent (as in β-TAnPD solid solutions) actinides. Previously published works show that monazites and β-TAnPD solid solutions present several similarities with regard to their preparation, their sintering process, and their dissolution. Both compounds could be prepared through the initial precipitation of low-temperature crystallized precursors:[14,25] during the heat treatment, these solids first dehydrate, leading to anhydrous compounds, and then turn into the final ceramic between 600 and 1000 °C. This transformation scheme can be applied to the preparation of sintered pellets by uniaxial pressing of the precursors at room temperature, and then firing between 1200 and 1400 °C.[14,25] The resulting ceramics appeared highly densified because the relative density lies between 95 and 98% of the calculated value for β-TUPD solid solutions and between 90 and 95% for the monazites.[14] Finally, these pellets present a strong resistance to aqueous alteration during leaching tests. For example, the normalized dissolution rate determined at 90 °C in a 10^{-1} M acidic solution (HCl or HNO_3) reaches about 1.1×10^{-4} g m^{-2} day^{-1} for β-TUPD solid solutions and 3.4×10^{-4} g m^{-2} day^{-1} for monazites.[14,25] Moreover, for both materials, the precipitation of neoformed phases in the back end of the initial dissolution process controls the solubility and induces the delay of the actinide's release in the solution. These phases were identified in each case for the precursor of the solid considered, uranium-depleted TUPHPH for β-TUPD and rhabdophane for monazite.[25,26]

This work reports the first results concerning the preparation, sintering, and chemical durability of β-TPD/monazite-based matrices. Tetravalent uranium simulated the incorporation of actinide(IV), whereas lanthanides were used as surrogates of trivalent actinides. Particularly, gadolinium was systematically incorporated in the solids, as the capability of several isotopes to absorb neutrons could prevent criticity problems in the case of the immobilization of large amounts of tetravalent plutonium in the β-TPD structure.

2. Experimental Section

2.1. Chemicals and Apparatus. Concentrated thorium chloride solutions ($C \approx 1.8$ M) were issued from Rhodia. The uranium chloride solution was obtained from the dissolution of uranium metal chips in 4 M hydrochloric acid. The initial solutions were diluted in order to obtain a final concentration of 0.7 M for thorium and 1.1 M for uranium(IV). The other chemical reagents used for syntheses and for analyses were from Aldrich and Fluka, and were of pro-analysis grade. The concentrations of the final solutions were determined using conventional analytical methods.

High-temperature treatments were performed in alumina boats in a Pyrox MDB 15 or HM 40 furnace up to 1200 °C with heating rates of 2−5 °C min^{-1}. To prevent the oxidation of uranium(IV) into uranyl, we performed all the heating treatments under an inert atmosphere (argon).

The XRD diagrams were collected with a Philips X'Pert-Pro PW 3040/60 or Bruker AXS-D8 Advance diffractometer system using Cu Kα rays (λ = 1.5418 Å). The precise peaks positions were determined using the fitting program EVA, available in the software package Diffrac-AT V 3.0, purchased by Socabim and supplied by Siemens.[27] Several diagrams were recorded for heating temperatures ranging from room temperature to 1100 °C under an inert

(11) Podor, R.; Cuney, M.; Nguyen Trung, C. *Am. Mineral.* **1995**, *80*, 1261−1268.
(12) Meldrum, A.; Boatner, L. A.; Weber, W. J.; Ewing, R. C. *Geochim. Cosmochim. Acta* **1998**, *62*, 2509−2520.
(13) Abraham, M. M.; Boatner, L. A.; Quinby, T. C.; Thomas, D. K.; Rappaz, M. *Radioact. Waste Manage.* **1980**, *1*, 181−191.
(14) Terra, O.; Clavier, N.; Dacheux, N.; Podor, R. *New J. Chem.* **2003**, *27*, 957−967.
(15) Benard, P.; Brandel, V.; Dacheux, N.; Jaulmes, S.; Launay, S.; Lindecker, C.; Genet, M.; Louër, D.; Quarton, M. *Chem. Mater.* **1996**, *8*, 181−188.
(16) Brandel, V.; Dacheux, N.; Genet, M. *Radiokhimiya* **2001**, *43*, 16−22.
(17) Dacheux, N.; Podor, R.; Chassigneux, B.; Brandel, V.; Genet, M. *J. Alloys Compd.* **1998**, *271*, 236−239.
(18) Dacheux, N.; Podor, R.; Brandel, V.; Genet, M. *J. Nucl. Mater.* **1998**, *252*, 179−186.
(19) Dacheux, N.; Thomas, A. C.; Brandel, V.; Genet, M. *J. Nucl. Mater.* **1998**, *257*, 108−117.
(20) Robisson, A. C.; Dacheux, N.; Aupiais, J. *J. Nucl. Mater.* **2002**, *306*, 134−146.
(21) Carpena, J.; Audubert, F.; Bernache, D.; Boyer, L.; Donazzon, B.; Lacout, J. L.; Senamaud, N. In *Scientific Basis for Nuclear Waste Management XXI*; Material Research Society: Boston, 1998.
(22) Podor, R. Synthèse et Caractérisation des Monazites Uranifères et Thorifères. Ph.D. Thesis, Université H. Poincaré−Nancy I, Vandoeuvre lès Nancy, France, 1994.
(23) Terra, O.; Audubert, F.; Dacheux, N.; Guy, C.; Podor, R. *J. Nucl. Mater.* Submitted.
(24) Terra, O.; Audubert, F.; Dacheux, N.; Guy, C.; Podor, R. In *Actinides−Basic Science, Applications and Technology*; Material Research Society: Boston, 2004.
(25) Clavier, N.; Dacheux, N.; Martinez, P.; Brandel, V.; Podor, R.; Le Coustumer, P. *J. Nucl. Mater.* **2004**, *335*, 397−409.
(26) Poitrasson, F.; Oelkers, E.; Schott, J.; Montel, J. M. *Geochim. Cosmochim. Acta* **2004**, *68*, 2207−2221.
(27) *Diffrac-AT*, version 3.1; Siemens: Berlin, 1991 (Socabim: Paris, 1986−1991).

atmosphere (nitrogen) using an HTK 1200 furnace from Anton Paar Instrument Company.

Electron probe microanalyses (EPMA) were carried out using a Cameca SX 50 apparatus with an acceleration voltage of 15 kV and a current of 10 nA considering the following calibration standards: $SmPO_4$ (Kα ray of phosphorus), ThO_2 (Mα ray of thorium), and UO_2 (Mβ ray of uranium). SEM micrographs were collected using a Hitachi S2500 scanning electron microscope equipped with Everhart−Ornley and in-lens SE detectors (only the former was used in our experiments). Electrons were supplied by a LaB_6 gun working at an acceleration voltage of 15 kV.

The dilatometer was a TMA 92-16 apparatus from Setaram working in an argon atmosphere from room temperature to 1300 °C. The relative experimental densities of the sintered samples were evaluated using water ($\rho = 0.997$ g cm^{-3} at 25 °C) after immersion and outgassing of the sample in the fluid or using helium pycnometry, whereas the determination of the dimensions of the pellets led to the geometric density. For measurements with helium, a multipycnometer from Quantachrome was used.

2.2. Leaching Tests. High-density polyethylene (HDPE) containers (showing low adsorption onto their surface) were used for performing the leaching experiments from 25 to 70 °C, whereas PTFE vessels were preferred for higher temperatures. After a washing step of the samples (10^{-1} M HNO_3 or HCl, 1−7 days) to avoid the presence of crystal defects, minor phases, or small particles that could induce perturbations for the determination of the normalized dissolution rates during the first days of the experiments, the leaching tests were conducted from 25 to 120 °C by mixing 100−200 mg of a sintered sample with 10 mL of acidic solution. A small volume of the leachate (100 μL) was taken, and was then renewed by fresh solution at regular intervals. After centrifugation of the sample at 13 000 rpm, we determined the concentrations of thorium and uranium in the leachate by inductively coupled plasma mass spectrometry using a Fisons Plasma Quad apparatus or by PERALS alpha liquid scintillation.[28] From these results, we determined the normalized leaching N_L (expressed in g m^{-2}) and the associated normalized dissolution rate R_L (in g m^{-2} day^{-1}) by considering the following equation

$$R_L(E_i) = \frac{dN_L(E_i)}{dt} = \frac{d}{dt}\left(\frac{C_{E_i} V M_{E_i}}{x_{E_i} S}\right) \quad (3)$$

where E_i = Th or U. In this expression, C_{E_i} corresponds to the concentration of the element E_i in the leachate, V to the volume of leachate, x_i to the mass ratio of E_i in the solid, and S to the effective surface area of the solid.

3. Results and Discussion

3.1. Preparation of the Precursors of β-TUPD/Monazite Matrices. The preparation of β-TUPD/monazite matrices involved the initial synthesis of low-temperature crystallized precursors, the final material being obtained after heating at high temperature. Indeed, pure β-TUPD solid solutions can be obtained by heating thorium−uranium (IV) phosphate hydrogen phosphate hydrate ($Th_{2-x/2}U_{x/2}(PO_4)_2(HPO_4)\cdot H_2O$, TUPHPH),[25] whereas monazites are prepared after firing rhabdophanes or hydrated monazites ($LnPO_4\cdot xH_2O$)[14,29] at high temperature. Two chemical routes based on precipitation processes were thus investigated to prepare the final ceramics.

In the so-called dry chemistry method, the precursors of each phase were precipitated separately. For both solids, acidic solutions containing cations U^{4+} and Th^{4+} for β-TUPD and Ln^{3+} for the monazites were mixed with concentrated phosphoric acid (5 M). Stoichiometric proportions of the reagents were introduced on the basis of the expected formula. However, an excess of 2% in moles of H_3PO_4 was used to ensure the quantitative precipitation of the cations. The mixtures were placed in PTFE closed containers, and were then heated on a sand bath for 1 week to a few months. During this step, the gelatinous phases that initially formed progressively turned into crystallized precipitates. The solids obtained were separated from the supernatant by centrifugation at 4000 rpm, washed several times with deionized water and then ethanol, dried in an oven (100 °C), and finally ground in a mortar. The rhabdophane was then heated in air up to 1300 °C to obtain the monazite form and to eliminate the remaining volatile products from the synthesis. Finally, the resulting monazite was mixed with TUPHPH by means of a mechanical grinding to prepare the precursor of the matrix.

The wet chemistry method started from the simultaneous precipitation of TUPHPH and rhabdophane. Mixtures of tetravalent actinides and trivalent lanthanides in hydrochloric solution were placed in PTFE containers and manually stirred, and then concentrated phosphoric acid was added dropwise. The mixture obtained generally turned into a gelatinous phase after a few seconds. This gel was finally transformed into a crystallized compound by heating on a sand bath for 1 week to 1 month at about 150 °C in a closed container. The solid was then treated following the same procedure as that described above.

3.2. Characterization of the Precursors. As the characterization of TUPHPH solid solutions[25,30,31] and of rhabdophanes[14,29,32] was already described, the physicochemical analyses were focused on samples prepared by the wet chemistry method in order to point out the eventual influence of the simultaneous precipitation on the properties of both phases.

First, the powder obtained after the simultaneous precipitation of tri- and tetravalent cations was characterized by XRD. The XRD pattern recorded for a mixture of $Th_{1.2}U_{0.8}(PO_4)_2(HPO_4)\cdot H_2O$ (60 wt %) and $GdPO_4\cdot 0.5H_2O$ (40 wt %) prepared at 150 °C during 1 week is reported in Figure 1, and is compared to that of pure TUPHPH (orthorhombic, *Cmcm* space group[33]) and of Gd−rhabdophane (hexagonal, $P3_121$ space group[34]). All the diffraction lines observed for the precursor belong to the TUPHPH or to the rhabdophane structures, showing that no additional peak is detected and

(28) Dacheux, N.; Aupiais, J. *Anal. Chem.* **1997**, *69*, 2275−2282.
(29) Jonasson, R. G.; Vance, E. R. *Thermochim. Acta* **1986**, *108*, 65−72.
(30) Dacheux, N.; Clavier, N.; Wallez, G.; Brandel, V.; Emery, J.; Quarton, M.; Genet, M. *Mater. Res. Bull.* **2005**, *40*, 2225−2242.
(31) Brandel, V.; Clavier, N.; Dacheux, N. *J. Solid State Chem.* **2005**, *178*, 1054−1063.
(32) Lucas, S. Synthèse et Comportement Thermique de Phosphates de Terres Rares Cériques ou Yttriques. Ph.D. Thesis, Université de Limoges, Limoges, France, 2003.
(33) Wallez, G.; Clavier, N.; Dacheux, N.; Quarton, M.; Van Beek, W. *Chem. Mater.* Submitted.
(34) Hezel, A.; Ross, S. D. *J. Inorg. Nucl. Chem.* **1967**, *29*, 2085−2089.

Table 1. Results of EPMA for a Mixture of $Th_{1.2}U_{0.8}(PO_4)_2(HPO_4)\cdot H_2O$ (60 wt %) and $Gd_{0.6}La_{0.2}Nd_{0.2}PO_4\cdot 0.5H_2O$ (40 wt %) Prepared by the Wet Chemistry Method ($T = 150$ °C, $t = 2$ weeks)

	U (wt %)	Th (wt %)	La (wt %)	Nd (wt %)	Gd (wt %)	P (wt %)	M/PO_4
phase I	23.6 ± 1.4	37.2 ± 0.5	NS[a]	0.2 ± 0.1	NS[a]	12.1 ± 0.1	0.67 ± 0.01
$Th_{1.2}U_{0.8}(PO_4)_2(HPO_4)\cdot H_2O$ calcd	24.6	36.0				12.0	0.67
phase II	0.8 ± 0.4	NS[a]	11.2 ± 0.6	10.3 ± 0.7	35.5 ± 1.3	12.9 ± 0.1	1.00 ± 0.01
$Gd_{0.6}La_{0.2}Nd_{0.2}PO_4\cdot 0.5\ H_2O$ calcd			10.9	11.3	37.0	12.2	1.00

[a] Not significant.

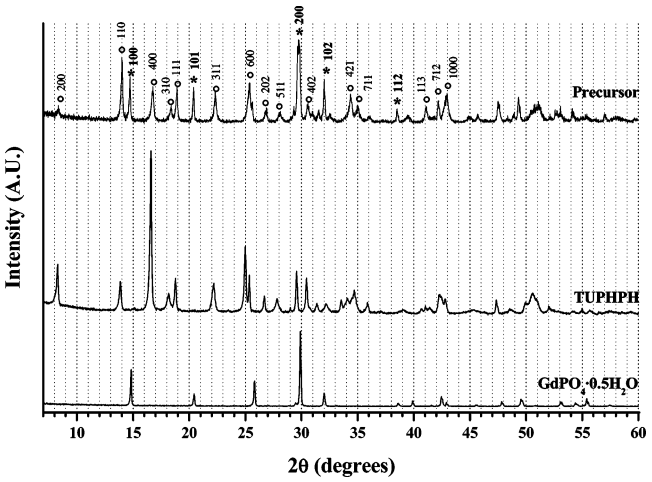

Figure 1. XRD pattern of a mixture of $Th_{1.2}U_{0.8}(PO_4)_2(HPO_4)\cdot H_2O$ (60 wt %) and $GdPO_4\cdot 0.5H_2O$ (40 wt %) prepared by the wet chemistry method ($T = 150$ °C, $t = 1$ week). XRD lines of TUPHPH (°) and rhabdophane (*). Indexations for Gd−rhabdophane are indicated in bold.

thus that no unexpected phase is formed during the precipitation process.

The exclusive presence of TUPHPH and rhabdophane in the samples prepared by the wet chemistry method was then checked through EPMA experiments (Table 1). For each phase, the elementary weight percents as well as the mole ratio of cations:PO_4 are found to be in good agreement with those values expected from the given formulas. Moreover, the segregation of tri- and tetravalent cations appears satisfying, as only small amounts of uranium and neodymium (less than 1 wt %) are found in the rhabdophane and in the TUPHPH phase, respectively.

Finally, the precursors prepared by the wet chemistry method were observed by SEM. The micrographs presented in Figure 2 clearly show two different morphologies. Multilayered aggregates about 20−30 μm in length (Figure 2a) can be attributed to the TUPHPH solid solution on the basis of X-ray energy dispersive spectroscopy (X-EDS) analyses. Gd−rhabdophane exhibits well-defined needlelike crystals 3−5 μm in length (Figure 2b), characteristic of its crystal structure.

3.3. Behavior of Precursors vs Temperature. The transformation of precursors into the high-temperature phases during heat treatment was followed by HT-XRD between room temperature and 1200 °C (Figure 3). The pattern recorded at 200 °C appeared similar to that described in the previous section for the raw powder, and corresponds to a mixture of TUPHPH and rhabdophane. Moreover, it remains unchanged between 200 and 800 °C, indicating that no significant structural modification occurs in this range of temperature. Nevertheless, because of the complexity of the diagrams and the weak differences between them, it is not possible to point out the successive transformations of TUPHPH into anhydrous TUPHP and then into α-TUPD,[33] which present closely related structures. Above 900 °C, the presence of additional XRD lines shows the transformation of α-TUPD into β-TUPD and Gd−rhabdophane into Gd−monazite. These transformations are found to be complete above 1000 °C, which appears to be consistent with the data reported in the literature for both phases.[29,30] Consequently, the simultaneous presence of α-TUPD and Gd−rhabdophane in the sample does not induce any modification of their behavior during the heat treatment. Above 1000 °C, the XRD

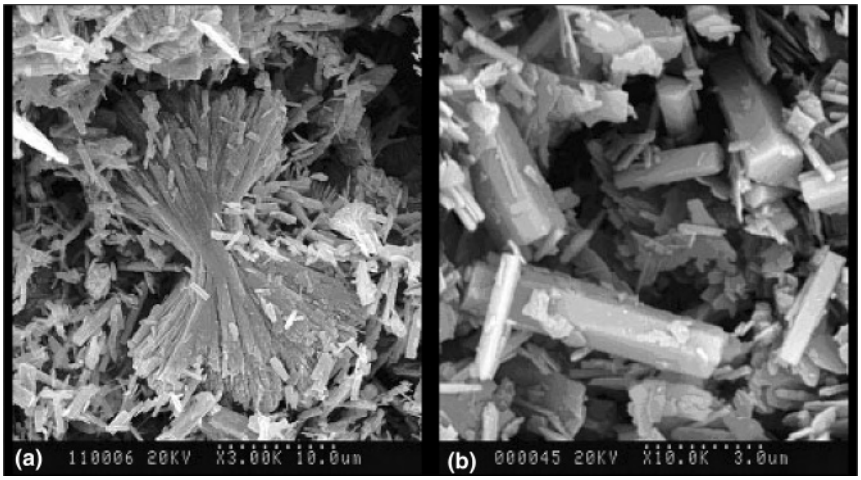

Figure 2. SEM observations of a mixture of $Th_{0.8}U_{1.2}(PO_4)_2(HPO_4)\cdot H_2O$ (85 wt %) and $GdPO_4\cdot 0.5H_2O$ (15 wt %) prepared by the wet chemistry method ($T = 150$ °C, $t = 1$ week).

Table 2. Results of EPMA for a β-$Th_{2.4}U_{1.6}(PO_4)_4P_2O_7$ (60 wt %)/$GdPO_4$ (40 wt %) Matrix (T = 1250 °C, t = 10 h)

	calcd values		dry chemistry method exp results		wet chemistry method exp results	
	β-$Th_{2.4}U_{1.6}P_6O_{23}$	$GdPO_4$	β-$Th_{2.4}U_{1.6}P_6O_{23}$	$GdPO_4$	β-$Th_{2.4}U_{1.6}P_6O_{23}$	$GdPO_4$
U (wt %)	25.5		23.7 ± 1.0	NS[a]	23.2 ± 0.5	3.4 ± 1.7
Th (wt %)	37.3		39.0 ± 0.5	NS[a]	36.4 ± 1.5	3.3 ± 1.6
Gd (wt %)		62.4	NS[a]	60.2 ± 1.5	1.7 ± 0.7	58.3 ± 1.1
P (wt %)	12.5	12.3	12.4 ± 0.1	12.5 ± 0.1	12.6 ± 0.1	12.5 ± 0.1
M/PO_4	0.67	1.00	0.67 ± 0.01	0.96 ± 0.02	0.65 ± 0.02	1.02 ± 0.02

[a] Not significant.

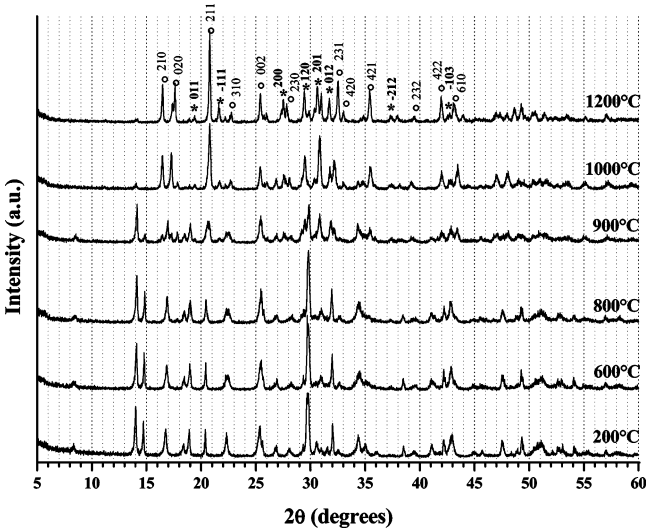

Figure 3. Variation of the XRD pattern of a mixture of $Th_{1.2}U_{0.8}(PO_4)_2(HPO_4)\cdot H_2O$ (60 wt %) and $GdPO_4\cdot 0.5H_2O$ (40 wt %) prepared by the wet chemistry method (T = 150 °C, t = 1 week). XRD lines of β-TUPD (°) and of Gd-monazite (*) indexations for Gd−monazite are indicated in bold.

pattern corresponds to a mixture of β-TUPD solid solution and Gd−monazite.

The unit cell parameters, refined from an HT-XRD diagram recorded at 1100 °C for both structures by means of the U-Fit software,[35] were found to be a = 12.785(5) Å, b = 10.390(3) Å, and c = 7.030(3) Å for the β-TUPD solid solution and a = 6.65(1) Å, b = 6.85(2) Å, c = 6.28(1) Å, and β = 104.3(3)° for Gd−monazite. These values appear to be in good agreement with those reported in the literature: a = 12.786(3) Å, b = 10.383(2) Å, and c = 7.027(2) Å,[36] and a = 6.6435(9) Å, b = 6.8414(10) Å, c = 6.3281(6) Å, and β = 103.98(1)°,[37] respectively. Moreover, no additional diffraction line is evident on the high-temperature diagram, showing that no chemical reaction leading to unexpected phases occurs between β-TUPD and monazite during the heat treatment.

The absence of an additional phase in the final material prepared above 1000 °C was also checked through EPMA experiments for both chemical routes (Table 2). Whatever the method considered, the elementary weight percents and the cation:phosphate mole ratios appear consistent with that expected from the formula. However, as was previously exposed for the low-temperature precursors, only the dry chemistry method allows for a complete segregation of tri- and tetravalent cations in the final materials. Indeed, for the wet chemistry method, 1.7 wt % gadolinium is incorporated in the β-TUPD solid solution whereas 3.3−3.4 wt % thorium and uranium are detected in the Gd−monazite structure. The second value appears to be similar to that reported in the literature when incorporating tetravalent cations by means of lacunar mechanisms in the monazite structure (up to 1 wt %),[22] whereas the β-TUPD structure could immobilize small quantities of trivalent elements (0.5 wt %).[38] Moreover, the slight shift induced in the elementary weight percents compared to that expected appeared to be similar to that observed for the precursors. Consequently, the incorporation of tetravalent actinides in the monazite and trivalent lanthanides in the β−TUPD should occur mainly during the precipitation step, and not through diffusion processes during the heat treatment.

3.4. Sintering of β-TUPD/Monazite Matrices. As the elaboration of dense pellets from low-temperature precursors was already reported for β-TUPD solid solutions,[39] we evaluated the influence of the monazite content on the sintering properties of the matrices. The densification of the pellets was obtained by means of a two-step procedure composed of a uniaxial pressing of the precursors at room temperature (100−800 MPa) and a heat treatment. For the solids prepared by the wet chemistry method, the initial powder was first heated at 400 °C for a few hours in order to eliminate the remaining volatile products (essentially water) coming from the synthesis.

The optimal conditions of sintering in terms of temperature and holding time for wet and dry chemistry methods were first determined by a dilatometric study (Figure 4).

Whatever the chemical process considered, the variation of the linear shrinkage vs the heat temperature occurs in three steps. The first relative linear shrinkage of about 1% recorded between 150 and 300 °C can be assigned to the full dehydration of rhabdophane and TUPHPH, and then to the transformation of TUPHPH into α-TUPD on the basis of the data reported for $La_{1-x}Gd_xPO_4$[14,29] and β-TUPD.[30] Because of the preliminary heat treatment achieved on the sample prepared by the wet chemistry method, this step is not observed in Figure 4a. The second significant relative shrinkage ($\Delta l/l$ of 3−4%) observed between 900 and 930 °C is correlated to the two phase transitions (Gd−rhabdophane → Gd−monazite and α-TUPD → β-TUPD). Both

(35) Evain, M. *U-Fit Program*; Institut des Matériaux de Nantes: Nantes, France, 1992.
(36) Dacheux, N. *PDF database: JCPDS file no. 50-1864*; International Centre for Diffraction Data: Newton Square, PA.
(37) Ni, Y. X.; Hughes, J. M.; Mariano, A. N. *Am. Mineral.* **1995**, *80*, 21−26.
(38) Thomas, A. C. Etude de la Dissolution du Phosphate-Diphosphate de Thorium. Ph.D. Thesis, Université Paris-Sud-11, Orsay, France, 2000.
(39) Clavier, N.; Dacheux, N.; Martinez, P.; du Fou de Kerdaniel, E.; Aranda, L.; Podor, R. *Chem. Mater.* **2004**, *16*, 3357−3366.

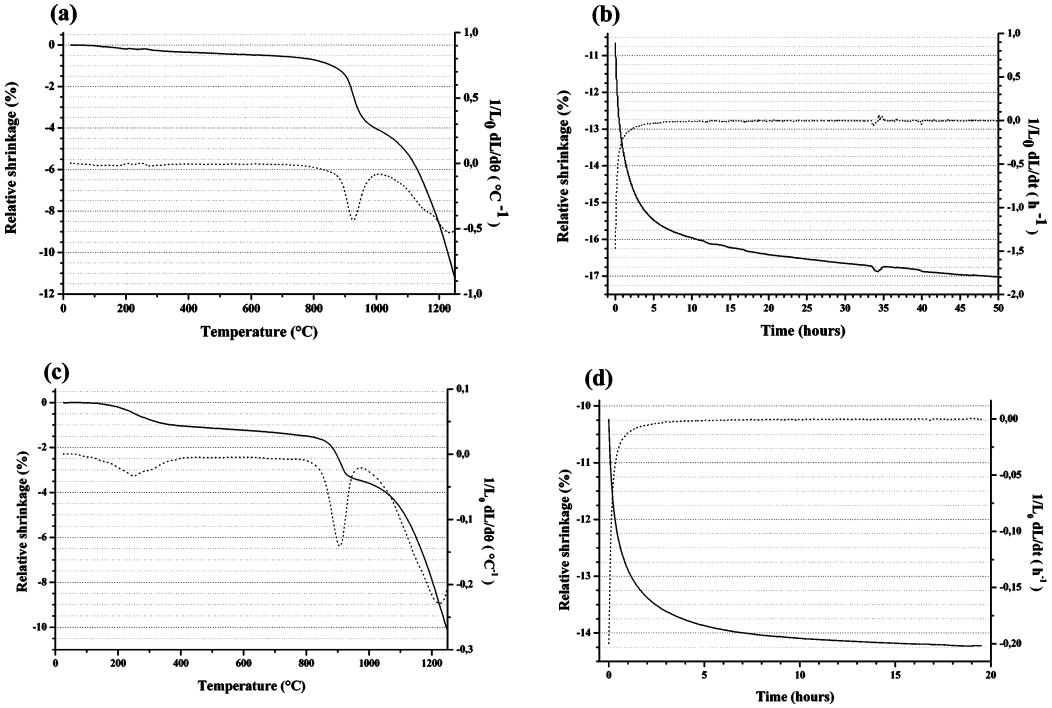

Figure 4. Variation in the dimensions of β-$Th_{2.4}U_{1.6}(PO_4)_4P_2O_7$ (85 wt %)/$GdPO_4$ (15 wt %) pellets prepared through wet (a and b) and dry (c and d) chemistry methods. Relative linear shrinkage and the derivatives are plotted by straight and dotted lines, respectively.

temperature ranges are not significantly modified compared to those of pure $La_{1-x}Gd_xPO_4$ (750 °C $\leq T \leq$ 950 °C) and TUPHPH (940 °C $\leq T \leq$ 960 °C) samples. Under these conditions, the thermal behavior of both phases seems to be independent of each other. Finally, the greater variation is recorded above 1100 °C ($\Delta l/l$ of 10−12%). This last step is associated with the densification of the material, and appears to be mainly due to the presence of a TUPHPH precursor.

While the chemical route seems to show no influence on the temperature of sintering, it appears to be of significant importance on the holding time required to achieve the sintering. Indeed, the mean relative shrinkage does not reach a plateau for the samples prepared by the wet chemistry method, showing that the sintering process goes on even after 50 h of heating (Figure 4b). On the contrary, only 10−20 h is necessary to perfect the densification of the samples prepared through the dry chemistry method ($\Delta l/l$ = 17%; Figure 4d). This observation is probably due to the presence of previously fired Gd−monazite (T = 1300 °C) in such samples, and is consistent with the densification of $La_{1-x}Gd_xPO_4$ monazites, which occurs at temperatures higher than 1250 °C.[14] From these results, the preparation of β-TUPD/monazite sintered pellets was performed using the dry chemistry method followed by a heat treatment for 10 h at 1250 °C to obtain the better densification state. The optimal operating conditions for the sintering of β-TUPD/monazite matrices were then checked by density measurements on pellets prepared by the dry chemistry method and fired at 1250 °C for various holding times (Table 3).

Whatever the amount of monazite considered, the density reached 91−96% of the calculated value after 10−20 h of heating, which corresponds to a global porosity of 4−9%. Consequently, the associated specific surface area is found to be very low (100−500 $cm^2\ g^{-1}$). From these results, it appears that the β-TUPD/monazite-based matrices are generally less densified than pure β-TUPD solid solutions.[39] This lower capability of sintering can be assigned to the presence of monazite in the solid because its optimal temperature of densification (above 1300 °C)[40] is higher than that used for this work. Indeed, the density of β-TUPD/monazite matrices is slightly deteriorated when the monazite amount in the solid is increased. However, highly densified compounds can be prepared by hot pressing performed at 1150 °C for 4 h under varying pressing conditions (15−30 MPa). For these operating conditions, the geometric density reaches 96% of the calculated value, whereas the apparent density is found to about 99%. These values correspond to a very low global porosity (less than 4%), and do not appear to be influenced by the monazite amount in the solid.

Table 3. Experimental Densities of Sintered β-$Th_{2.4}U_{1.6}(PO_4)_4P_2O_7$/$La_{0.4}Ce_{0.4}Gd_{0.2}PO_4$ Matrices (dry chemistry method, T = 1250 °C)[a]

holding time (h)	15 wt % monazite		40 wt % monazite		70 wt % monazite	
	d_{geom}	d_{exp}	d_{geom}	d_{exp}	d_{geom}	d_{exp}
2	4.84 (91)	4.89 (92)	4.74 (90)	4.84 (91)	4.68 (88)	4.81 (90)
4	4.84 (91)	4.92 (93)	4.80 (91)	4.87 (92)	4.70 (89)	4.82 (91)
6	4.90 (92)	4.93 (93)	4.86 (92)	4.89 (93)	4.80 (90)	4.82 (91)
8	4.93 (93)	4.95 (93)	4.84 (91)	4.89 (93)	4.78 (90)	4.83 (91)
10	4.91 (93)	4.97 (94)	4.85 (91)	4.91 (93)	4.79 (91)	4.85 (91)
20	4.96 (94)	4.99 (95)	4.93 (93)	4.97 (94)	4.88 (92)	4.91 (93)

[a] Relative error of 2%. Values in parentheses are percentages of calcd density for β-$Th_{2.4}U_{1.6}(PO_4)_4P_2O_7$/$La_{0.4}Ce_{0.4}Gd_{0.2}PO_4$ matrices, which is 5.31.

SEM micrographs showed the densification of the material after heating at 1250 °C (Figure 5): a lot of grain boundaries are observed, whereas only a few pores of 1−2 μm diameter

(40) Bregiroux, D.; Lucas, S.; Champion, E.; Audubert, F.; Bernache-Assollant, D. *J. Eur. Ceram. Soc.* **2006**, *26*, 279−287.

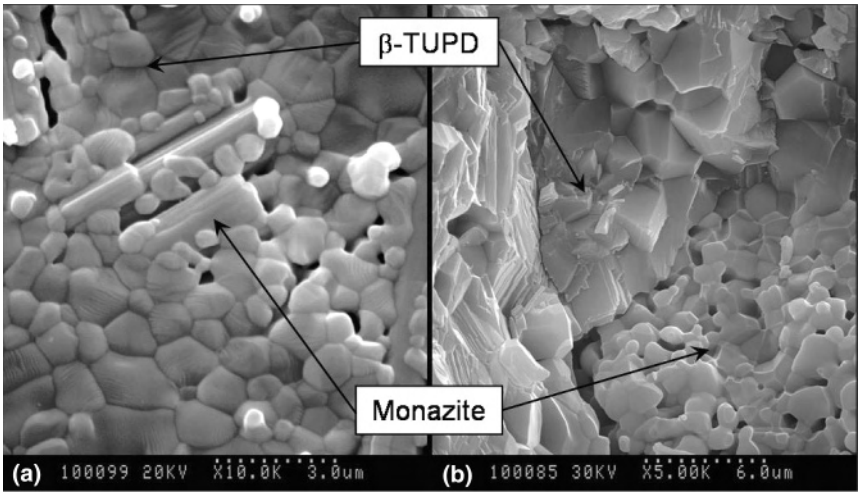

Figure 5. SEM micrographies of a sintered β-$Th_{2.4}U_{1.6}(PO_4)_4P_2O_7$ (85 wt %)/$GdPO_4$ (15 wt %) pellet (dry chemistry method, $T = 1250$ °C, $t = 20$ h).

Table 4. EPMA Results for β-$Th_{2.4}U_{1.6}(PO_4)_4P_2O_7$/$La_{0.4}Ce_{0.4}Gd_{0.2}PO_4$ Matrices (dry chemistry method, $T = 1250$ °C, $t = 20$ h)

	U (wt %)	Th (wt %)	La (wt %)	Ce (wt %)	Gd (wt %)	P (wt %)	M/PO_4	phase
				Calcd Values				
β-TUPD	25.5	37.3				12.5	0.67	I
monazite			23.4	23.5	13.2	13.0	1.00	II
				Exp Values				
15 monazite wt %	24.1 ± 0.9	37.2 ± 0.8	NS[a]	NS[a]	NS[a]	12.8 ± 0.2	0.64 ± 0.02	I
	1.3 ± 0.5	NS[a].	21.5 ± 0.9	22.4 ± 0.7	14.0 ± 0.4	12.9 ± 0.1	1.01 ± 0.01	II
40 monazite wt %	23.4 ± 0.5	38.6 ± 0.4	NS[a]	NS[a]	NS[a]	12.7 ± 0.1	0.65 ± 0.01	I
	1.3 ± 0.6	NS[a]	21.4 ± 0.6	22.2 ± 0.8	14.4 ± 0.6	12.8 ± 0.2	1.01 ± 0.02	II
70 monazite wt %	23.1 ± 0.9	38.9 ± 0.9	NS[a]	NS[a]	NS[a]	13.0 ± 0.3	0.64 ± 0.02	I
	0.9 ± 0.4	NS[a]	21.9 ± 0.9	22.5 ± 0.7	14.7 ± 0.7	12.8 ± 0.1	1.02 ± 0.01	II

[a] Not significant.

are detected at the surface (Figure 5a). The predominant role of the monazite in the porosity of the final material is also evident, as the porosity appears to be mainly located in two different zones. At the surface of the pellets, open pores are formed at the interphase between β-TUPD (spherical grains) and monazite (needlelike grains) and are probably due to the difference in the sintering rate of the two phases. The bulk material (Figure 5b) clearly exhibits large differences in the sintering of the solid. X-EDS analyses allowed for identifying the zones of more highly closed porosity to monazite.

Despite its influence on the densification, the presence of monazite during the sintering process does not influence the chemical composition of the final ceramics. Whatever the amount of monazite in the solid, EPMA experiments led to elementary weight percents and mole ratios consistent with that expected (Table 4).

However, a small part (around 1 wt %) of tetravalent cations, mainly uranium, is incorporated in the monazite structure. Because the two phases are initially precipitated separately in the dry chemistry process, the incorporation probably occurs through diffusion processes during the heat treatment, with the reactivity of the powders being increased by the pressing step. Nevertheless, X-EDS observations performed on these sintered samples allow for pointing out the good segregation of tri- and tetravalent cations in the β-TUPD/monazite matrices (Figure 6). Thorium appears almost totally located in the β-TUPD phase (in light gray on the BSE micrograph), whereas lanthanum is fully incorporated in monazite (in dark gray in the BSE micrograph). These observations confirm the importance of monazite on the final density of the material, as the porosity appears to be mainly located in monazite aggregates, which also degrades the homogeneity of the pellet. Under these conditions, the improvement of the homogeneity of the final solids should significantly enhance the global density by surrounding small monazite grains with dense β-TUPD. Some experiments are now being developed with this objective.

3.5. Study of the Chemical Durability of the Samples. The chemical durability of β-TUPD/monazite radwaste matrices was evaluated through leaching tests in acidic media. First, the kinetic aspect of the dissolution was considered in order to evaluate the influence of monazite on the normalized leaching rate. The neoformed phases precipitated in the back end of the initial dissolution process, which thermodynamically control the concentrations of ions in the leachate, were then extensively characterized.

The normalized leaching rates $R_L(U)$, determined from the amount of uranium in the leachate (Table 5), appear to be in good agreement with those previously reported for pure β-TUPD solid solutions.[41] Indeed, for pH = 1, the $R_L(U)$ value varies from $(8.2 \pm 0.7) \times 10^{-6}$ to $(2.7 \pm 0.4) \times 10^{-2}$ g m^{-2} day^{-1} between 25 and 120 °C for β-TUPD/monazite matrices, whereas the values were found to be between 2.5×10^{-5} and 2.3×10^{-3} g m^{-2} day^{-1} for β-TUPD. Moreover,

(41) Dacheux, N.; Clavier, N.; Ritt, J. *J. Nucl. Mater.* In press.

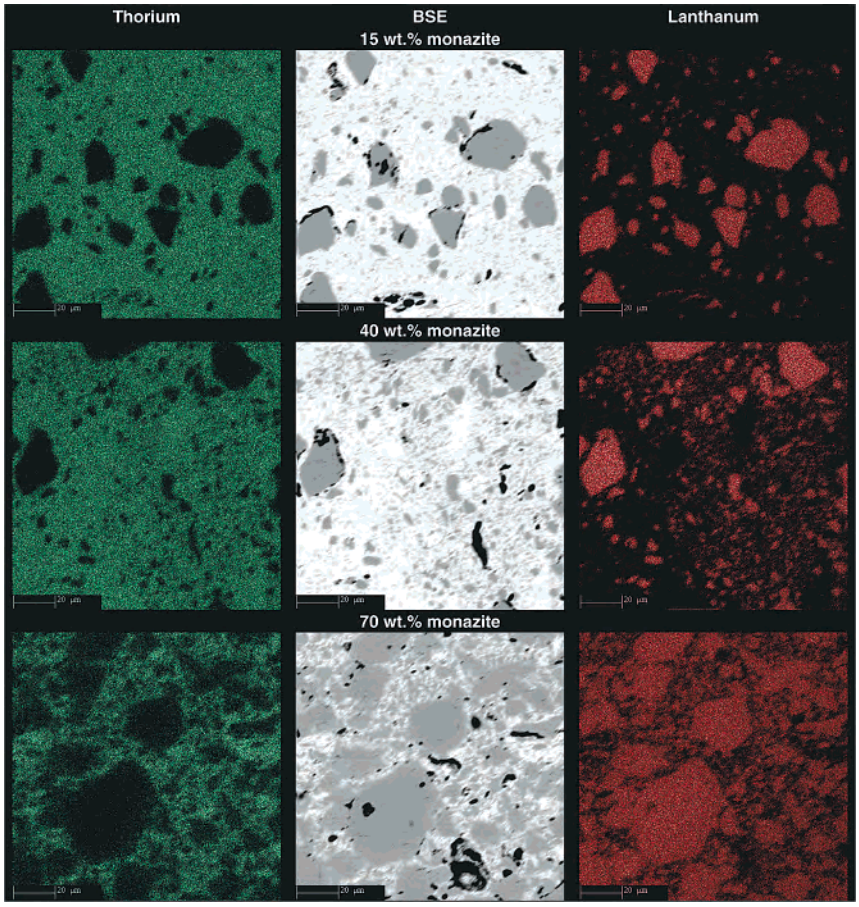

Figure 6. X-EDS mapping of β-$Th_{2.4}U_{1.6}(PO_4)_4P_2O_7$/$La_{0.4}Ce_{0.4}Gd_{0.2}PO_4$ matrices (dry chemistry method, $T = 1250$ °C, $t = 20$ h).

Table 5. ICP-MS Results for the Leaching of β-$Th_{2.4}U_{1.6}(PO_4)_4P_2O_7$ (60 wt %)/$La_{0.8}Nd_{0.1}Gd_{0.1}PO_4$ (40 wt %) in 10^{-1} M HNO_3 ($T = 90$ °C)

time (days)	C_U (M)	C_{Th} (M)	C_{La} (M)	C_{Nd} (M)	C_{Gd} (M)
1	5.7×10^{-5}	3.1×10^{-6}	9.7×10^{-7}	1.9×10^{-6}	9.1×10^{-7}
5	2.0×10^{-4}	8.0×10^{-6}	3.3×10^{-6}	2.8×10^{-6}	2.2×10^{-6}
9	2.6×10^{-4}	1.0×10^{-6}	3.8×10^{-6}	1.7×10^{-6}	2.8×10^{-6}
13	2.7×10^{-4}	6.7×10^{-7}	3.3×10^{-6}	1.3×10^{-6}	2.3×10^{-6}
21	3.8×10^{-4}	1.8×10^{-6}	3.2×10^{-6}	1.1×10^{-6}	2.4×10^{-6}
36	7.0×10^{-4}	ND[a]	ND[a]	ND[a]	ND[a]
55	1.0×10^{-3}	<LD[b]	5.0×10^{-6}	3.9×10^{-6}	<L.D.
85	1.7×10^{-3}	<LD[b]	4.1×10^{-6}	3.3×10^{-6}	<L.D.
108	2.8×10^{-3}	<LD[b]	<LD[b]	<LD[b]	4.0×10^{-7}
191	3.8×10^{-3}	<LD[b]	<LD[b]	<LD[b]	<LD[b].
257	4.9×10^{-3}	ND[a]	ND[a]	ND[a]	ND[a]
296	4.1×10^{-3}	ND[a]	ND[a]	ND[a]	ND[a]
376	5.1×10^{-3}	ND[a]	ND[a]	ND[a]	ND[a]
480	4.3×10^{-3}	<LD[b]	<LD[b]	<LD[b]	<LD[b].

[a] Not determined. [b] Below the limit of detection.

these values appear very low by comparison to several other materials studied in the same aim, such as borosilicate glasses.[42] On the basis of the dissolution rates collected at various temperatures and from the following equation

$$R_L(E_i) = ke^{-E_A/RT} \quad (4)$$

an approximate value of the activation energy of the dissolution reaction was evaluated to be about 48 ± 6 kJ mol^{-1}. Although these results include an important uncertainty due to the low normalized dissolution rates observed, especially at room temperature, this value appears to be consistent with those determined for pure β-TUPD and monazites,[43] and agrees well with the dissolution mechanism, based on surface reactions,[44] proposed for these solids.

Moreover, the behavior of tetravalent cations in the β−TUPD/monazite matrices appears similar to that described for β-TUPD solid solutions:[45] uranium is released in the leachate, probably due to its oxidation in the UO_2^{2+} uranyl ion, whereas thorium is precipitated as a neoformed phase (Figure 7, Table 5). This precipitation occurs quickly for pH > 1, leading to an incongruent dissolution. For pH = 1, the dissolution first appears congruent, and the precipitation then takes place after several days to a few weeks, depending on the temperature considered. Consequently, the normalized dissolution rates were mainly determined from the amount of uranium in the leachate, because the thorium concentration leads to nonsignificant values (see Table 6). Trivalent cations are also found to precipitate quickly as neoformed phases in the back end of the initial dissolution process. Under these conditions, all the normalized dissolution rates determined from the concentration of lanthanides in the leachate appeared very low, and complicate the comparison with the data

(42) Frugier, P.; Martin, C.; Ribet, I.; Advocat, T.; Gin, S. *J. Nucl. Mater.* **2005**, *346*, 194−207.
(43) Oelkers, E.; Poitrasson, F. *Chem. Geol.* **2002**, *191*, 73−87.
(44) Lasaga, A. C. *Rev. Mineral.* **1995**, *31*, 23−86.
(45) Clavier, N.; du Fou de Kerdaniel, E.; Dacheux, N.; Le Coustumer, P.; Drot, R.; Ravaux, J.; Simoni, E. *J. Nucl. Mater.* In press.

Table 6. Normalized Leaching Rates Determined for β-$Th_{2.4}U_{1.6}(PO_4)_4P_2O_7$ (85 wt %)/$La_{0.8}Nd_{0.1}Gd_{0.1}PO_4$ (15 wt %) in 10^{-1} M HNO_3 at Various Temperatures

	R_L(i) (g m^{-2} day^{-1})				
T (K)	U	Th	La	Gd	Nd
298	$(8.2 \pm 0.7) \times 10^{-6}$	$(1.1 \pm 0.6) \times 10^{-5}$	$(1.2 \pm 0.3) \times 10^{-7}$ [b]	$(7.3 \pm 0.7) \times 10^{-7}$ [b]	$(6.1 \pm 0.5) \times 10^{-7}$ [b]
363	$(3.5 \pm 0.1) \times 10^{-4}$	$(3.5 \pm 0.7) \times 10^{-4}$	$(1.7 \pm 1.4) \times 10^{-6}$ [b]	$(3.1 \pm 0.4) \times 10^{-7}$ [b]	NS[a]
393	$(2.7 \pm 0.4) \times 10^{-3}$	$(2.5 \pm 0.8) \times 10^{-6}$ [b]		NS[a].	

[a] Not significant. [b] Quick precipitation of thorium in neoformed phosphate-based phases.

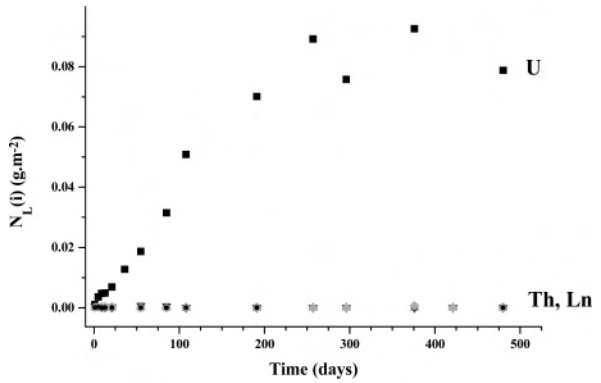

Figure 7. Evolution of normalized losses N_L(Th) (●), N_L(U) (■), and N_L(Ln) (◆, La; ▼, Nd; ▲, Gd) for sintered β-$Th_{2.4}U_{1.6}(PO_4)_4P_2O_7$ (60 wt %)/$La_{0.8}Nd_{0.1}Gd_{0.1}PO_4$ (40 wt %) in 10^{-1} M HNO_3 (T = 90 °C).

reported in the literature for monazites.[43] Nevertheless, the precipitation of lanthanide ions was often described under operating conditions close to those employed in this work.[14,26]

Taking into account the precipitation of thorium and lanthanide ions in the back end of the dissolution, we investigated the surface of leached β-TUPD/monazite pellets by SEM (Figure 8). The micrographs clearly allow for the identification of two different morphologies corresponding to the neoformed phases. From X-EDS analyses, multilayered aggregates of about 5−10 μm were found to contain thorium and a small part of the remaining tetravalent uranium. This agrees well with the results obtained during the dissolution of pure β-TUPD, for which the solubility of tetravalent actinides in the leachate is controlled by the precipitation of strongly uranium-depleted TUPHPH solid solution.[45]

Consequently, the multilayered aggregates observed during the dissolution of β-TUPD/monazite matrices were identified as T(U)PHPH solid solution. On the other hand, several needlelike crystals 10 μm in length are observed at the surface of the leached pellet, and are found to contain only trivalent lanthanides from X-EDS analyses. Because lanthanide phosphate ($LnPO_4 \cdot nH_2O$) can precipitate as three different crystalline forms, i.e., monazite, rhabdophane, and xenotime (quadratic, I41/amd),[46] depending on the average ionic radius and the temperature considered,[47] it appeared difficult to precisely characterize the nature of the neoformed phase. However, because of the lanthanide ions considered in our experiments, the precipitation of a xenotime could be excluded, this phase being prepared only for heavy rare earth elements (mainly from holmium to lutetium[14]), and the morphology of the crystals seems to indicate the precipitation of the rhabdophane form. Also, the concentrations measured in the leachate at equilibrium (10^{-1} M HNO_3, T = 90 °C) in lanthanides, $[Ln^{3+}] = 9 \times 10^{-6}$ M, and in free phosphate ions, $[PO_4^{3-}] = 4.5 \times 10^{-23}$ M, lead to a solubility product $pK_s = 27.4$, which is in very good agreement with the values generally reported for rhabdophane and monazite[26] (we can report, for instance, the value obtained by Oelkers et al. for neodymium phosphate: $pK_s = 27.7$). Finally, on the basis of the previous studies,[48] we expected uranyl to precipitate for longer leaching times than the uranyl phosphate pentahydrate $(UO_2)_3(PO_4)_2 \cdot 5H_2O$.[49]

Under these conditions, the presence of such neoformed phases at the surface of the leached pellets should significantly delay the release of actinides in the leachate, as was observed for β-TUPD.[45] Moreover, these precipitated phases allow for conserving the complete segregation between tri- and tetravalent cations already observed in the β-TUPD/monazite matrices prepared through the dry chemistry method.

4. Conclusion

Several samples of β-TUPD/monazite-based radwaste matrices were prepared through two different chemical routes. The first was based on the simultaneous precipitation of crystallized precursors of each phase. The second started from the individual precipitation of these solids, the initial calcination of rhabdophane in order to get monazite, and finally a mechanical mixing of the phases. For both methods, β-TUPD/monazite matrices were obtained after heating these precursors above 1000 °C. No additional phase was detected in the final compound by either XRD or EPMA, showing that the phases did not react together. Moreover, the presence of monazite did not affect the chemical scheme of transformation of TUPHPH into β-TUPD. The distribution of the cations in the solid was carefully studied for both methods. It appeared that only the dry chemistry route allowed for the complete segregation of tri- and tetravalent cations, as a small amount of lanthanides was found in the β-TUPD structure and few actinides were incorporated in the monazite for the wet chemistry method.

The sintering of these matrices was then performed through a rather simple two-step procedure based on a uniaxial pressing at room temperature and a heat treatment

(46) Milligan, W. O.; Mullica, D. F.; Beall, G. W.; Boatner, L. A. *Inorg. Chim. Acta* **1983**, *70*, 133−136.
(47) Clavier, N. Elaboration de Phosphate−Diphosphate de Thorium et d′Uranium (β-PDTU) et de Matériaux Composites β-PDTU/Monazite à Partir de Précurseurs Cristallisés. Etudes du Frittage et de la Durabilité Chimique. Ph.D. Thesis, Université Paris-Sud-11, Orsay, France, 2004.
(48) Thomas, A. C.; Dacheux, N.; Le Coustumer, P.; Brandel, V.; Genet, M. *J. Nucl. Mater.* **2001**, *295*, 249−264.
(49) Saadi, M.; Dion, C.; Abraham, F. *J. Solid State Chem.* **2000**, *150*, 72−80.

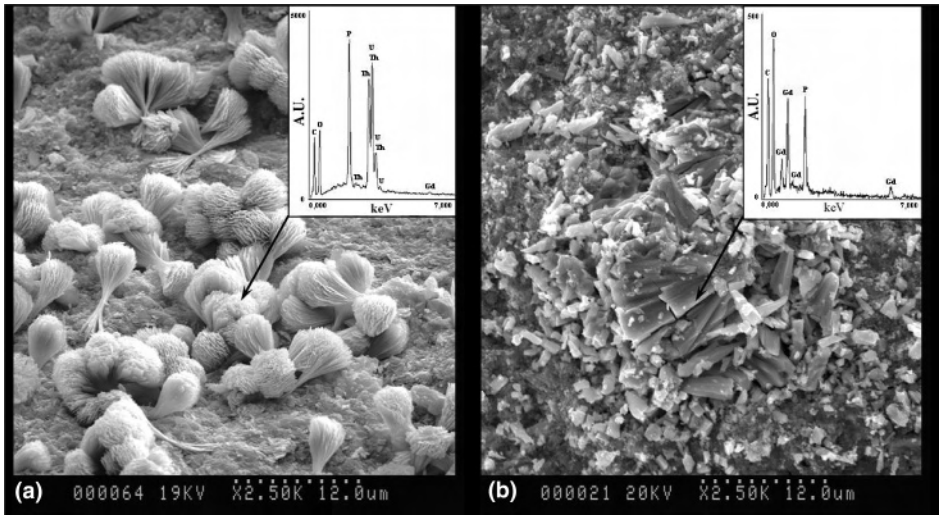

Figure 8. SEM observations of neoformed phases precipitated onto leached β-$Th_{2.4}U_{1.6}(PO_4)_4P_2O_7$ (85 wt %)/$GdPO_4$ (15 wt %) (10^{-1} M HNO_3, $T = 90$ °C, $t = 3$ months).

at high temperature. From dilatometric experiments, the optimal temperature of sintering was found to be 1250 °C for both chemical routes. Besides, it appeared that the densification was more effective for the dry method, as only 10−20 h of heat treatment was required compared to more than 50 h for the wet chemistry method. In the optimal conditions set from these results, the relative densities of the pellets reached 90−95% of the calculated value, which appeared to be slightly lower than that for pure β-TUPD solid solutions. This lower capability to sinter came from the presence of monazite in the solid, as the porosity was found to be located mainly in this phase (close porosity) or at the interphase between β-TUPD and monazite (open porosity).

Finally, the chemical durability of β-TUPD/monazite sintered pellets was evaluated by leaching tests in acidic media. The first results showed a good resistance to aqueous alteration, with the normalized dissolution rates ranging from $(8.2 \pm 0.7) \times 10^{-6}$ to $(2.7 \pm 0.4) \times 10^{-2}$ g m^{-2} day^{-1} between 25 and 120 °C at pH = 1. Moreover, these values are in good agreement with those previously reported for β-TUPD solid solutions, which seems to indicate that the presence of monazite does not affect the chemical durability of the solid. Also, different behaviors were oberved in the leachate depending on the cation considered: uranium was released in solution because of its oxidation in the uranyl form, whereas thorium and lanthanides were quickly precipitated as neoformed phosphate-based phases. These phases were identified at the surface of the pellet as uranium-depleted T(U)PHPH solid solutions for thorium and as rhabdophane or monazite for lanthanides. Under these conditions, the presence of these phases could significantly delay the release of cations in the leachate, and thus to the biosphere.

From all these results, β-TUPD/monazite radwaste matrices appeared to be potential good candidates for the simultaneous immobilization of tri- and tetravalent actinides. Complementary experiments are actually in progress to improve the synthesis and sintering steps to obtain denser and more homogeneous solids. Several leaching tests will also be performed in basic, acidic, and neutral media in order to give a multiparametric expression of the normalized dissolution rate. Finally, compounds of high specific activity will be prepared by incorporating plutonium, neptunium, or americium. The results of such studies could allow for the application of the precipitation of β-TUPD/monazite precursors to the effective decontamination of radioactive liquid waste containing actinides.

Acknowledgment. This work was supported by the French Research Group NOMADE (GdR 2023). The authors thank Lionel Aranda, Johann Ravaux, Jean-Paul Emeraux, and Alain Kohler from the LCSM of the University Henri Poincaré—Nancy I (France) for performing EPMA, dilatometric experiments, HT-XRD, and SEM observations. They are also grateful to Jerôme Ritt from IRSN, Fontenay-Aux-Roses (France), for his support during the ICP-MS measurements.

IC051607P